Supporting Information

Impact of Organic Hole Transporting Material and Doping on the Electrical Response of Perovskite Solar cells

Maria Ulfa,[a] Thierry Pauporté,[a]* Thanh-Tuân Bui,[b] Fabrice Goubard[b],

[a] Chimie ParisTech, PSL Research University, CNRS, Institut de Recherche de Chimie Paris (IRCP), 11 rue P. et M. Curie, F-75005 Paris, France

[b] Laboratoire de Physicochimie des Polymères et des Interfaces, Université de Cergy-Pontoise, 5 mail Gay Lussac, 95000 Neuville-sur-Oise, France.

* Corresponding author: thierry.pauporte@chimie-paristech.fr

A. Oxidation mechanisms of Spiro-OMeTAD.

The oxidation of Spiro-OMeTAD is required to get a HTM suitable for PSC application. Compared to its pristine form, the oxidized one has a conductivity higher by several orders of magnitude. Oxidized Spiro-OMeTAD is characterized by an absorption band in the 450-550 nm spectral range and can then be followed by spectrophotometry.

The oxidation mechanism of Spiro-OMeTAD was first studied in relation to the solid-state dye-sensitized solar cell (ssDSSC) application. Different oxidation mechanisms have been proposed in the literature. They can be direct, by a strong oxidant or by molecular oxygen. In the latter case, the assistance of annealing, additives, light and/or acids is required

The effect of light was first proposed by Bach and coll. for ssDSSCs.[1] In their mechanism, electrons coming from excited dyes are captured by oxygen and the oxidized Spiro-OMeTAD is created by regeneration of the oxidized dye. In the reactions, LiTFSI functions either as a catalyst or a stabilizer of the oxidized Spiro-OMeTAD. The mechanism is written as:

$$Dye + h\nu \rightarrow Dye^* \rightarrow Dye^+ + e^-(TiO_2) \quad (S1)$$

$$e^-(TiO_2) + O_2 \rightarrow O_2^{\bullet -} \quad (S2)$$

$$Dye^+ + \text{Spiro-OMeTAD} \rightarrow Dye + \text{Spiro-OMeTAD}^{\bullet +} \quad (S3)$$

A similar mechanism has been suggested later for PSCs by Wang et al..[2] They have shown a wavelength dependent mechanism. Spiro-OMeTAD can be directly oxidized as a radical cation by O_2 using short wavelength radiations:

$$\text{Spiro-OMeTAD} + O_2 + h\nu \rightarrow \text{Spiro-OMeTAD}^{\bullet+}O_2^{\bullet-} \quad \text{(S4)}$$

$$\text{Spiro-OMeTAD}^{\bullet+}O_2^{\bullet-} + Li^+TFSI^- \rightarrow \text{Spiro-OMeTAD}^{\bullet+}TFSI^- + Li_xO_y \quad \text{(S5)}$$

Whereas, for long wavelength radiations (>450 nm), a three step mechanism would occur:

$$\text{Perovskite} + O_2 + h\nu\ (>450\ \text{nm}) \rightarrow \text{Perovskite}^+O_2^{\bullet-} \quad \text{(S6)}$$

$$\text{Perovskite}^+O_2^{\bullet-} + \text{Spiro-OMeTAD} \rightarrow \text{Perovskite} + \text{Spiro-OMeTAD}^{\bullet+}O_2^{\bullet-} \quad \text{(S7)}$$

$$\text{Spiro-OMeTAD}^{\bullet+}O_2^{\bullet-} + Li^+TFSI^- \rightarrow \text{Spiro-OMeTAD}^{\bullet+}TFSI^- + Li_xO_y \quad \text{(S8)}$$

On the other hand, Snaith et al. have described the oxidation of Spiro-OMeTAD without light and dye/perovskite assistance.[3] They have proposed a two-step mechanism: first, the formation of an oxidized SpiroOMeTAD from equilibrium between Spiro OMeTAD with O_2 (S9). Second, by adding LiTFSI, the balance is disturbed, because the superoxide radical $O_2^{\bullet-}$ reacts with Li^+ to form Li_2O and Li_2O_2, and finally Spiro-OMeTAD$^{\bullet+}$TFSI$^-$ is generated (S10).

The mechanism could be written as:

$$\text{Spiro-OMeTAD} + O_2 \leftrightarrow \text{Spiro-OMeTAD}^{\bullet+}O_2^{\bullet-} \quad \text{(S9)}$$

$$\text{Spiro-OMeTAD}^{\bullet+}O_2^{\bullet-} + \text{LITFSI} \rightarrow \text{Spiro-OMeTAD}^{\bullet+}TFSI^- + Li_xO_y \quad \text{(S10)}$$

Li et al. have stated that the latter reaction is slow.[4] Adding an acid, such as H_3PO_4, accelerates the reaction and favors the oxidation in the presence of LiTFSI. Moreover, NaTFSI, which is inactive without acid, becomes active and promotes the oxidation reaction in the presence of acid.

Fang et al.[5] have reported the activation of Spiro-OMeTAD oxidation in the presence of LiTFSI by annealing at 80°C and, better, at 140 °C.

In the case of Co(III) complex dopants, the oxidation of Spiro-OMeTAD has been described as direct with the direct and rapid formation of the radical cation.[6] Using a Co(III) complex with a

higher redox potential (by playing on the ligands) favors the oxidation reaction. They have also shown that Co(II) complexes are inactive.[6]

$$\text{Spiro-OMeTAD} + [\text{Co(III)}]_{\text{complex}} \rightarrow \text{Spiro-OMeTAD}^{\bullet+} + [\text{Co(II)}]_{\text{complex}} \qquad \text{(S11)}$$

References

(1) Cappel, U. B.; Daeneke, T.; Bach, U. Oxygen-Induced Doping of Spiro-MeOTAD in Solid-State Dye-Sensitized Solar Cells and Its Impact on Device Performance. *Nano Lett*. **2012**, *12*, 4925-4931

(2) Wang, S.; Yuan, W.; Meng, Y.S. Spectrum-Dependent Spiro-OMeTAD Oxidization Mechanism in Perovskite Solar Cells. *ACS Appl. Mater. Interfaces* **2015**, *7*, 24791−24798.

(3) Abate, A.; Leijtens, T.; Pathak, S.; Teuscher, J.; Avolio, R.; Errico, M.E.; Kirkpatrik, J.; Ball, J.M.; Docampo, P.; McPherson, I. at al. Lithium Salts as "Redox Active" p-Type Dopants for Organic Semiconductors and their Impact in Solid-State Dye-Sensitized Solar Cells. *Phys. Chem. Chem. Phys*. **2013**, *15*, 2572-2579.

(4) Li, Z.; Tinkham, J.; Schulz, P.; Yang, M.; Kim, D.H; Berry, J.; Sellinger, A.; Zhu K. Acid Additives Enhancing the Conductivity of Spiro-OMeTAD Toward High-Efficiency and Hysteresis-Less Planar Perovskite Solar Cells. *Adv. Energy Mater*. **2017**, *7*, 1601451.

(5) Fang, Y.; Wang, X.; Wang, Q.; Huang, J.; Wu, T. Impact of Annealing on Spiro-OMeTAD and Corresponding Solid-State Dye Sensitized Solar Cells. *Phys. Status Solidi A* **2014**, *211*, 2809–2816.

(6) Burschka, J.; Kessler, F.; Nazeeruddin, M.K.; Grätzel, M. Co(III) Complexes as p-Dopants in Solid-State Dye-Sensitized Solar Cells. *Chem. Mater*. **2013**, *25*, 2986-2990.

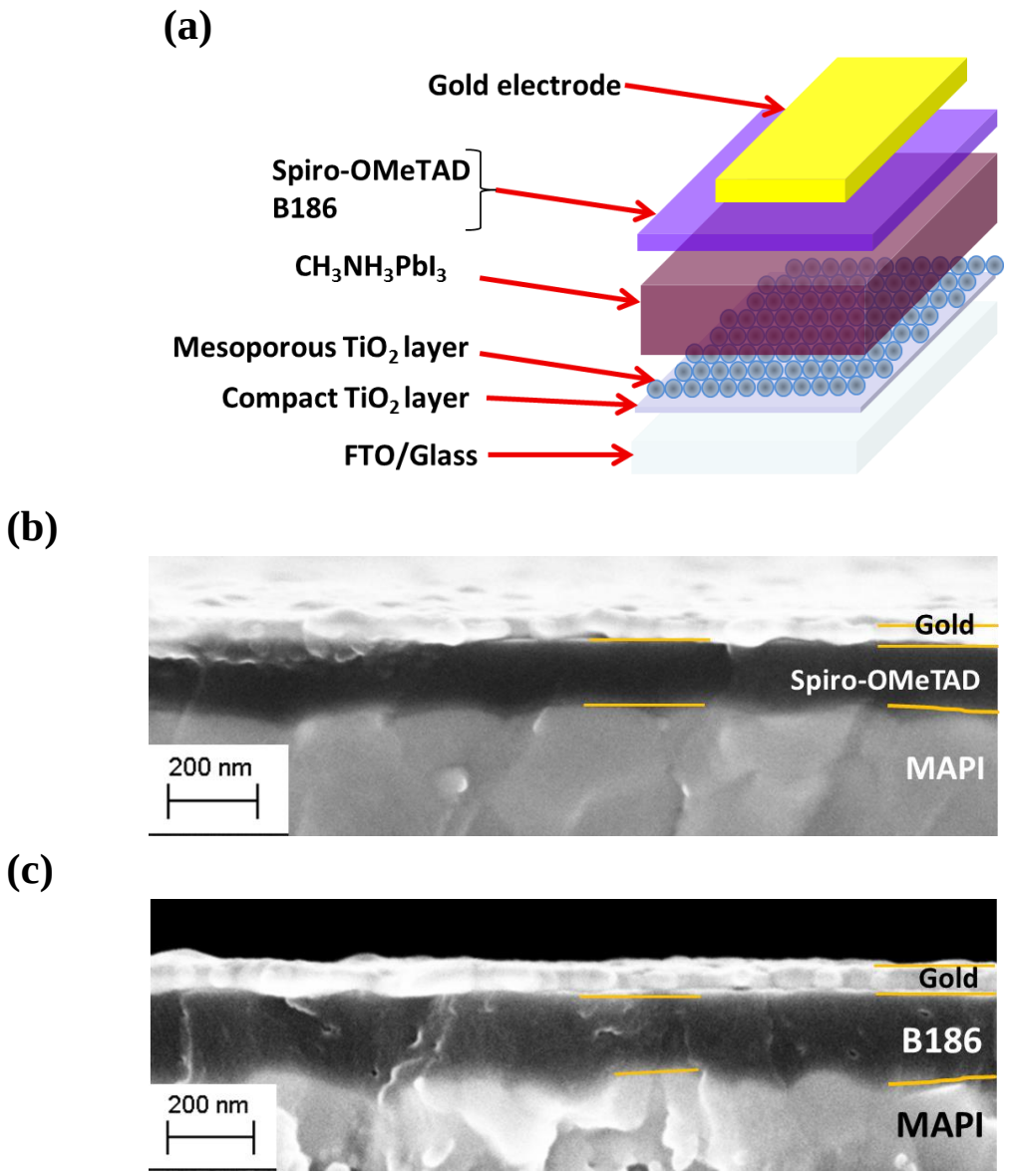

Figure S1. (a) Exploded schematic view of the perovskite solar cells. (b) SEM cross-sectional views of Spiro-OMeTAD and (c) B186 layers.

Table S1. Effect of the HTM and doping on the photovoltaic *J-V* curve parameters of the investigated cells (AM1.5 solar spectrum irradiated at 100 mW.cm^{-2}). The numbers in brackets are the standard deviations.

HTM	Doping	Scan direction		V_{oc} / V	J_{sc}/ mA.cm^{-2}	FF/ %	PCE/ %
Spiro-OMeTAD	Doped	Rev[a]	Best[c]	1.01	22.15	78.22	17.68
			Avg[d]	1.01 (0.02)	20.83 (0.63)	76.5 (2.70)	16.10 (1.00)
		For[b]	Best	1.00	22.72	63.02	14.45
			Avg	0.987 (0.02)	21.02 (1.06)	59.3 (2.91)	12.42 (1.22)
	Undoped Oxidized	Rev	Best	0.93	16.41	42.61	6.55
			Avg	0.903 (0.030)	15.14 (0.88)	37.13 (7.46)	5.13 (1.31)
		For	Best	0.920	15.35	26.80	3.79
			Avg	0.865 (0.059)	13.84 (1.13)	22.26 (2.59)	2.70 (0.57)
	Undoped	Rev	Best	0.94	16.67	32.62	5.13
			Avg	0.910 (0.031)	12.61 (3.58)	27.24 (8.71)	3.46 (1.95)
		For	Best	0.94	16.44	26.55	4.10
			Avg	0.908 (0.028)	12.07 (3.62)	21.66 (5.41)	2.59 (1.37)
B186	Doped	Rev	Best	0.98	20.11	73.27	14.59
			Avg	0.96 (0.03)	19.60 (1.33)	70.40 (3.00)	13.44 (0.91)
		For		0.92	20.27	33.76	6.33
			Avg	0.92 (0.02)	19.80 (1.39)	33.80 (8.01)	6.33 (1.79)
	Undoped	Rev	Best	0.74	1.52	16.89	0.19
			Avg	0.73 (0.016)	1.31 (0.27)	16.31 (0.37)	0.16 (0.03)
		For	Best	0.74	1.44	16.64	0.17
			Avg	0.73 (0.013)	1.41 (0.27)	16.26 (0.32)	0.164 (0.029)

[a] Measured in the reverse bias scan direction; [b] measured in the forward bias scan direction. [c] Best cells; [d] Avg: averaged values.

B. General electrical equivalent circuit and its simplifications.

For the analysis of the impedance data, the spectra have been fitted with equivalent electrical circuits (EECs). The general EEC employed is presented in Figure S2. However, except for the undoped Spiro-OMeTAD cells, all the components of this circuit could not be observed and analyzed on the spectra. Therefore, simplified circuits have been used. They are noted Type I, Type II and Type III in Figure S2.

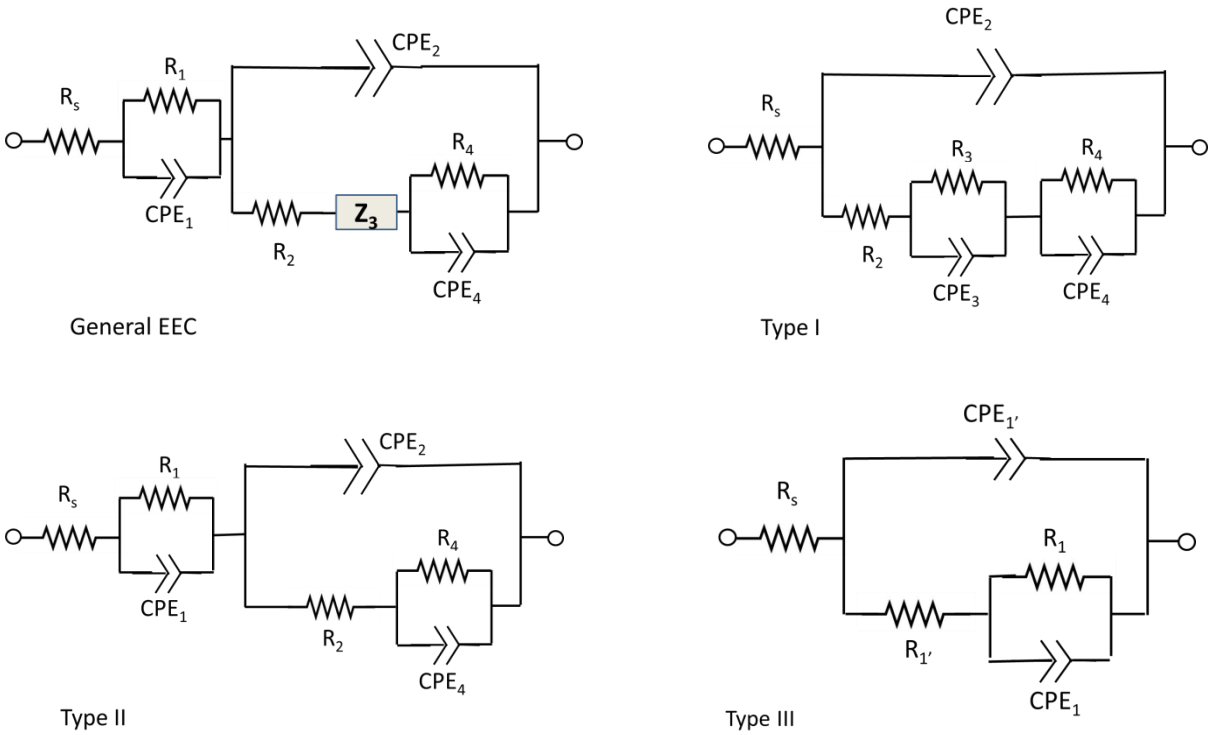

Figure S2. General equivalent electrical circuit (EEC) and different types of simplified EECs employed to fit the impedance spectra of the perovskite solar cells measured under light at various voltages.

For the *Doped*-**Spiro** cells, the very high frequency loop 1 was not observed and a R_3//CPE_3 circuit was used as Z_3 to fit the small arc of circle present at the foot of the low frequency loop. The low frequency component was noted 4 and fitted with a R_4//CPE_4 circuit. The same simplified circuit was used in the case of *Doped*-**B186** cells. For undoped B186 cells, the low frequency points were not analyzed and the type III circuit with two relaxations was employed to fit the flattened arc of circle. The 1 and 1' components are labelled in Figure 2c. The 1 component is assigned to the electrical response of the bulk B186 layer, whereas we have not been able to identify the origin of 1' component at the present time. In the case of the oxidized Spiro-OMeTAD cells, the Z_3 component was not seen and the spectra were fitted with the type II ECC.

Table S2 summarizes the various EEC types used to analyze the various kinds of PSC spectra.

Table S2. EECs employed to fit the impedance spectra of cells prepared with various HTM.

	HTM	Equivalent electrical circuit
Doped	Spiro-OMeTAD	Type I
	B186	
oxidized	Spiro-OMeTAD	Type II
Undoped	Spiro-OMeTAD	General
	B186	Type III

Table S3. *J-V* curve parameters of the analyzed $FA_{0.87}MA_{0.13}Pb(I_{0.87}Br_{0.17})_3$ PSCs using B186 and Spiro-OMeTAD HTMs.

	Scan direction	V_{oc} / V	J_{sc}/ mA.cm^{-2}	FF/ %	PCE/ %
B186 with Co	Rev	1.03	20.21	69.23	14.45
	For	0.98	20.19	62.69	12.42
SpiroOMeTAD	Rev	1.00	20.47	78.72	16.09
	For	0.98	20.40	65.01	13.09

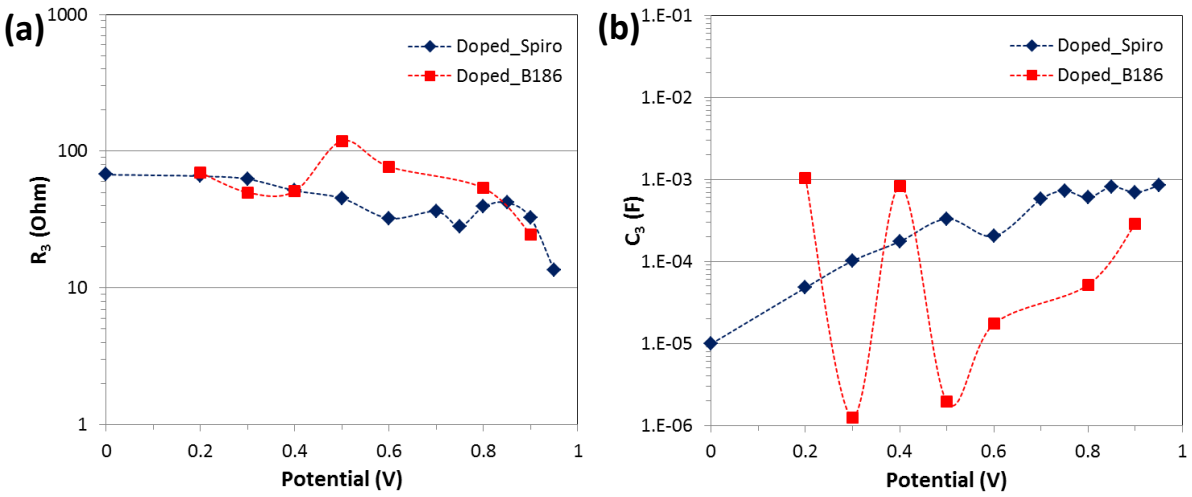

Figure S3: Effect of HTM and doping on C_3 (a) and R_3 (b) parameters measured at various applied potentials.

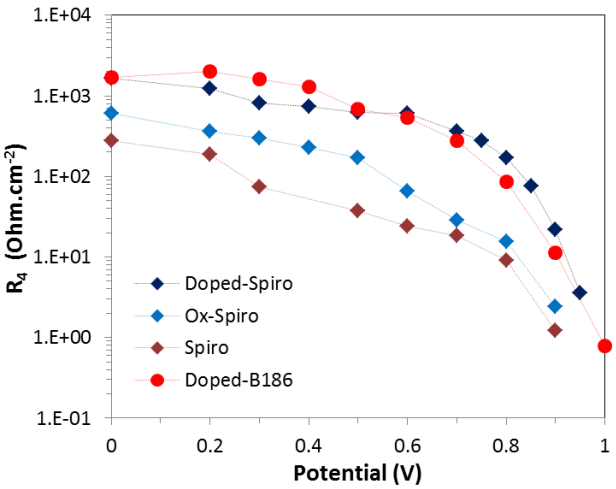

Figure S4: Effect of HTM and doping on R_4 parameter measured at various applied potentials.

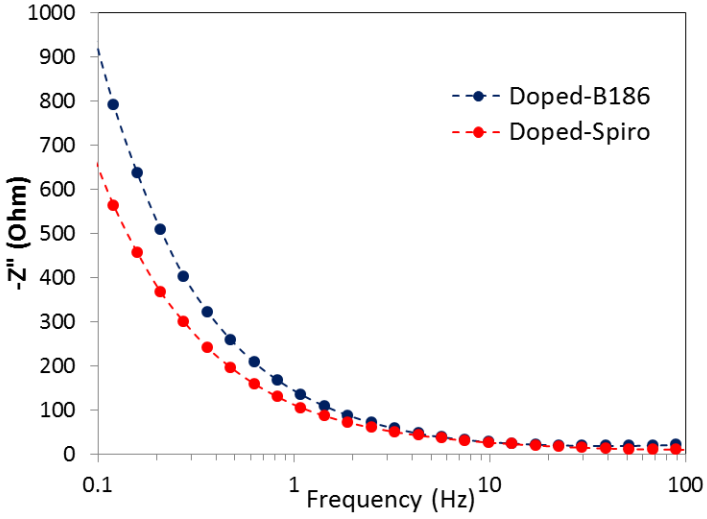

Figure S5: Plot of the imaginary part (Z") of the impedance versus the frequency for the doped-HTM cells.